Multi-scale characterization of tumor-draining lymph nodes in resectable lung cancer treated with neoadjuvant immune checkpoint inhibitors

Haitang Yang,[a,1] Beibei Sun,[b,1] Wenyan Ma,[c,1] Liwen Fan,[a,1] Ke Xu,[a] Yunxuan Jia,[a] Jianlin Xu,[d]* Zhexin Wang,[a]* and Feng Yao [a,e]*

[a]Department of Thoracic Surgery, Shanghai Chest Hospital, Shanghai Jiao Tong University; Shanghai, China
[b]Institute for Thoracic Oncology, Shanghai Chest Hospital, Shanghai Jiao Tong University; Shanghai, China
[c]Clinical Research Center, Shanghai Chest Hospital, Shanghai Jiao Tong University, Shanghai, China
[d]Department of Respiratory Medicine, Shanghai Chest Hospital, Jiao Tong University; Shanghai 200030, China
[e]Wenzhou Medical University, Wenzhou, China

eBioMedicine 2022;84: 104265
Published online xxx
https://doi.org/10.1016/j.ebiom.2022.104265

Summary

Background Regional lymph node (LN) acts as a pivotal organ for antitumor immunity. Paradoxically, tumor-draining LNs (TDLNs) are usually the first site of tumor metastasis in lung cancer. It is largely unknown about the association between the status of TDLNs and the response of primary tumor beds to immune checkpoint inhibitors (ICIs) in lung cancer patients. Also, studies characterizing the TDLNs in response to ICIs are scarce.

Methods We characterized and compared the radiological, metabolic (18F-FDG) and pathologic responses between primary tumor beds and paired TDLNs (invaded/non-invaded) from 68 lung cancer patients who underwent neoadjuvant ICIs plus surgery. Additionally, we performed the spatial profiling of immune and non-immune cells within TDLNs using multiplexed immunofluorescence. Therapy responses (e.g., pathologic complete (pCR) or major response (MPR)) of primary lung tumor beds and paired TDLNs were investigated separately.

Findings We observed that responses of TDLNs to ICIs markedly differ from their paired primary lung tumors regarding the radiological, metabolic (18F-FDG uptake), and pathologic alterations. Neoadjuvant ICIs therapy specifically decreased 18F-FDG-reflected metabolic activity in the primary tumor beds with pCR/MPR but not their TDLNs counterparts. Furthermore, the presence of invaded TDLNs was associated with poor pathologic responses in the matched primary tumor beds and predictive of rapid post-treatment tumor relapse. Spatial profiling demonstrated exclusion of T cell infiltrates within the metastatic lesions of invaded TDLNs, and diminished multiple immune and non-immune compositions in non-involved regions surrounding the metastatic lesions.

Interpretation These results provide the first clinically-relevant evidence demonstrating unique response patterns of TDLNs under ICIs treatment and revealing the underappreciated association of TDLNs status with the response of their paired primary tumors to ICIs in lung cancer.

Funding This work was supported by the National Natural Science Foundation of China (82072570 to F. Yao; 82002941 to B. Sun), the excellent talent program of Shanghai Chest Hospital (to F.Y), the Basic Foundation Program for Youth of Shanghai Chest Hospital (2021YNJCQ2 to H.Yang), and the Innovative Research Team of High-level Local Universities in Shanghai (SHSMU-ZLCX20212302 to F. Yao).

Keywords: Lung cancer; Immune checkpoint inhibitors; Neoadjuvant immunotherapy; Tumor-draining lymph nodes; Pathologic response; Biomarker

*Corresponding authors at: Shanghai Chest Hospital, Shanghai Jiao Tong University, West Huai 241, Shanghai 200030, China.
E-mail addresses: yanghaitang@shchest.org (H. Yang), xujianlin@shchest.org (J. Xu), wzx1953@shchest.org (Z. Wang), yaofeng@shsmu.edu.cn (F. Yao).

[1] H.Y., B.S., W.M., and L.F. contributed equally to this work.

Research in context

Evidence before this study

Immunotherapy has profoundly changed the treatment paradigm for patients with lung cancer. However, heterogeneous therapy responses exist, which can be caused by various factors, e.g., cancer cell itself or tumor microenvironment. Although considerable biomarkers have been identified to stratify patients who may benefit from the immune checkpoint inhibitors (ICIs) treatment, their performance varies from patient to patient. Thus, there is still a growing need to understand the pathobiology of tumor evasion from immune surveillance and elucidate the mechanisms of drug action, ultimately facilitating tailored treatment.

It is a long-held notion that the regional draining lymph nodes (LN), enriched for various immune components, act as pivotal organs for antitumor immunity. Recent evidence also demonstrates tumor-draining LNs (TDLNs) as a reservoir of tumor-specific T cells, driving their infiltration into the primary tumors. However, TDLNs are frequently observed as the first site of tumor metastasis in lung cancer. The underlying molecular mechanisms that promote the adaption of cancer cells to the immune-proficient microenvironment within TDLNs remain to be explored. Particularly, the impact of TDLNs status (tumor-free vs. tumor-invaded) on the response of their primary tumors to ICIs treatment in lung cancer patients is largely unknown. Furthermore, studies characterizing the spatial profiling of the immune and non-immune compositions between the invaded and paired non-invaded TDLNs in the context of ICIs treatment are lacking.

Added value of this study

Neoadjuvant ICIs therapy, followed by surgery, provides an ideal situation to simultaneously evaluate the therapeutic responses of primary tumors and paired TDLNs to ICIs. Based on a clinical cohort of lung cancer patients undergoing neoadjuvant ICIs plus surgery, we first characterized and compared the clinicopathological characteristics of patients who had good or poor responses. Strikingly, our work showed that cases with poor response to neoadjuvant ICIs treatment were mostly associated with more tumor-invaded TDLNs, and the presence of invaded TDLNs was identified as the only independent biomarker predicting the therapeutic response of their paired primary tumors. These observations indicate that invaded TDLNs might render a restrained antitumor immunity despite the activation under ICIs treatment. More importantly, the presence of invaded TDLNs was predictive of rapid tumor relapse in these patients after neoadjuvant ICIs treatment, suggesting that the residual tumor cells within the invaded TDLNs might represent a special subset, which is not only able to escape the immune surveillance and resist ICIs treatment but also is a critical source of tumor recurrence. Further, spatial profiling revealed a remarkable difference in the immune and non-immune compositions between the invaded and the paired non-invaded TDLNs, providing certain interpretations for the compromised therapy response associated with the invaded TDLNs.

Implications of all the available evidence

Our findings highlighted the presence of metastatic TDLN as a previously underappreciated biomarker predictive of ICIs response and as a potentially critical source of ICIs treatment failure, which advances our knowledge of the importance of TDLNs-mediated local immunity to effective immunotherapy. Particularly, this might be instrumental to guide the rationalized design of improved immunotherapies in the clinic. For instance, systematic/unselected removal of TDLNs is a clinical routine for surgical treatment of lung cancer. Instead, our findings support the precise/selected removal of invaded TDLNs while leaving the non-invaded TDLNs intact to improve the therapeutic outcomes of subsequently adjuvant ICIs treatment, given that TDLNs are critical sites for antitumor immunity and the generation of an effective response to ICIs. Also, strategies using TDLNs-directed local therapy combined with systematic ICIs may provide more therapeutic benefits.

Introduction

Immune checkpoint inhibitors (ICIs) have greatly revolutionized the treatment of various cancer types at late stages, including lung cancer. Recent evidence also highlighted the promises of neoadjuvant ICIs followed by surgery in resectable lung cancer.[1] Nonetheless, clinical evidence has demonstrated heterogeneous responses in patients receiving ICIs, and primary or secondary therapy resistance is common.[2] These observations suggest an urgent need to understand the pathobiology of the immunotherapy failure to guide better management of ICIs in the clinic.

Cytotoxic T cells are the fundamental effectors in the antitumor immune response and form the backbone of effective cancer immunotherapies. Previously, ICIs were presumed to work by directly reinvigorating exhausted CD8+ T Cells that pre-exist within the tumor microenvironment. However, emerging evidence highlighted the importance of newly primed and expanded effector T cells outside of the tumor microenvironment that play a key role in mediating the antitumor response.[3,4] One of the most critical sources is the regional tumor-draining lymph nodes (TDLNs) that are highly enriched for T cells and other immune components and play an essential role in antitumor immunity.[5] Specifically, antigen-presenting cells, e.g., dendritic cells, capture tumor antigens in the primary tumor tissues and then migrate to the TDLNs, where T cells are subsequently primed. Ultimately, primed T cells infiltrate into the primary tumor sites and mediate tumor eradication. Mounting evidence has highlighted

the necessity of various components within TDLNs for the efficacy of ICIs, including the immune and non-immune cells within TDLNs,[3,6,7] which, however, was mainly based on pre-clinical mouse models of other cancer types with a lack of clinical evidence on lung cancer. Moreover, most of these preclinical studies focused on the tumor-uninvolved TDLNs, whereas the impact of involved TDLNs on tumor immunity remains to be defined.

The lung is a highly immunological organ rich in multiple stations of draining lymph nodes.[8,9] Paradoxically, tumor cells metastasizing to TDLNs have been frequently observed, either macroscopically or microscopically, in surgically-resected lung cancer cases despite the absence of detectable distant dissemination,[10] and the presence of metastatic TDLNs is also proposed as a strong dismal prognosis factor.[11] Consistently, previous preclinical models and recent single-cell-based lineage tracing analyses support the local lymphatic system as an early metastatic route of lung cancer, prior to distant metastasis.[12-14] These phenomena appear to challenge the presumably classical anti-tumor functions of TDLNs. Supporting this notion, systematic dissection of TDLNs is a standard surgical procedure, leading to improved survival of patients with resectable lung cancer.[15,16] Furthermore, in pre-clinical models, recent evidence also showed a tumor-promoting role of TDLNs in cancer progression.[17,18] Together, these observations suggested that TDLNs execute complex and seemingly contradictory functions during tumor pathogenesis. Therefore, the role of TDLNs in shaping tumor immunity warrants further studies, particularly in the scenario of ICIs treatment whose efficacy is closely related to the immune and non-immune cells within the TDLNs.[3,19–22]

Pathologic complete response (pCR) or major response (MPR) in the primary tumor beds is a widely-accepted surrogate marker for the therapeutic benefits and survival prediction for lung cancer patients after neoadjuvant ICIs[1,23]; however, the therapeutic response in the TDLNs has not been well characterized.[24] Particularly, whether the presence of invaded/metastatic TDLNs (referred to as TDLNs+) affects the treatment response in the primary tumor beds remains elusive.

Thus, in the present study, to characterize and compare the therapeutic responses between primary tumors and their paired TDLNs, as well as reveal the potential biological role of TDLNs in mediating the efficacy of ICI treatment, we separately characterized and compared the therapeutic responses of the primary tumor beds with their paired TDLNs in patients with locally-advanced lung cancer who underwent neoadjuvant ICIs plus surgery. Interestingly, we observed markedly different response patterns concerning changes in the radiographical size, metabolic activity, and pathologic responses between the primary tumor beds and their paired TDLNs. Strikingly, the presence of TDLNs+ independently predicts poor response to ICIs in the primary tumor beds, with more TDLNs+ being associated with a higher frequency of poor therapy response. Spatial profiling using multiplexed immunofluorescence (mIF) staining revealed differential profiling of immune and non-immune compartments between TDLNs+ and their paired non-invaded TDLNs (referred to as TDLNs-). Collectively, our data demonstrated unique response patterns of TDLNs under ICIs treatment and revealed the underappreciated association of TDLNs status with the response to neoadjuvant ICIs in lung cancer, which might facilitate our treatment decision-making.

Methods

Study design and patients

Clinicopathological data of patients with locally-advanced non-small cell lung cancer (NSCLC) (clinically staged as $T_xN_{1-3}M_0$ or $T_{3-4}N_xM_0$ (x stands for any stages)) who received neoadjuvant immunotherapy or chemo-immunotherapy followed by surgery were retrieved from the clinical records. The study design was summarized in Figure 1.

Ethics statements for animal experiments

This study was approved by the institutional review board of Shanghai Chest Hospital (#KS(Y)22139). All patients had signed informed consent for inclusion of their clinical data and specimens in the institutional Lung Biobank and use in research projects, according to the recommendation of the institutional review board. The study was conducted in accordance with the Declaration of Helsinki (as revised in 2013).

Experimental reagents and antibodies

The reagents and antibodies used were listed in Table S1.

Pretreatment and preoperative examinations

The clinical stage of patients who received neoadjuvant treatment was assessed by positron emission tomography with 2-deoxy-2-[fluorine-18] fluoro-D-glucose integrated with computed tomography (18F-FDG PET-CT) scan or other whole-body examinations. Detailed information regarding the pretreatment and preoperative examinations were shown in the Supplemental Methods.

The measurement of radiographic size and metabolic activity of abnormal TDLNs

Abnormal TDLNs were defined as TDLNs with pathologically-confirmed metastasis by pre-treatment biopsy of regional nodes ($N = 28$) or radiological suspicion of regional nodal metastasis ($N = 40$) indicated by the size (shortest diameter $\geq$ 10 mm) and/or elevated pre-treatment maximum standardized uptake value (SUVmax) on 18F-FDG PET-CT scan. If there are multiple

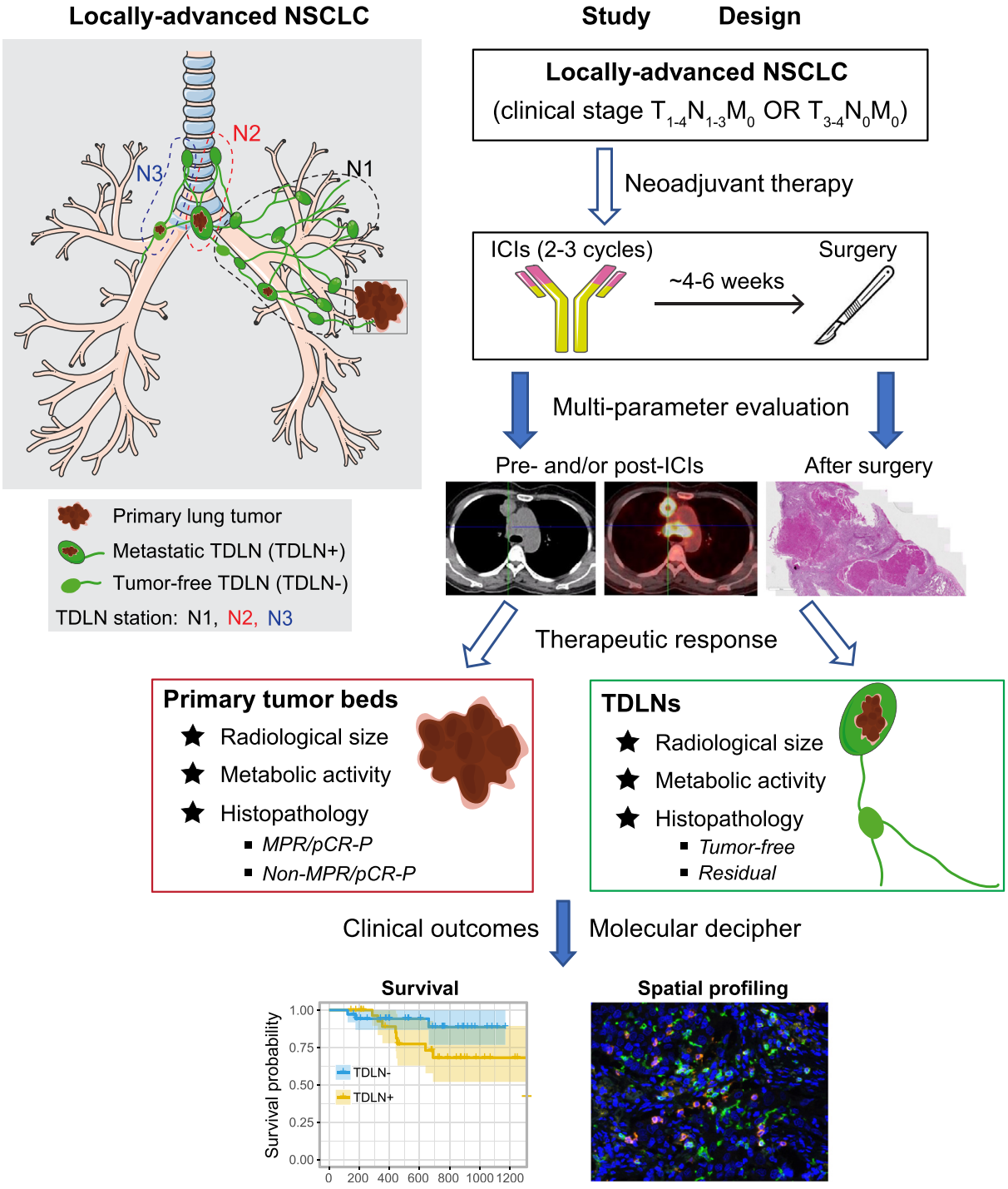

Figure 1. Study design. Patients with locally-advanced non-small cell lung cancer (NSCLC) who received neoadjuvant immune checkpoint inhibitors (ICIs) followed by surgery were included. Separately analyzing the therapeutic responses, e.g. radiological size, metabolic activity (reflected by 18F-FDG PET-CT), and the degree of pathologic response, were performed in primary tumor beds and paired tumor-draining lymph nodes (TDLNs). Additionally, we divided the TDLNs into two groups according to their pathologic status: TDLNs with residual tumor cells (metastatic; TDLN+) and tumor-free TDLNs (TDLN-). Multi-parameters between the TDLNs+ and TDLNs- were then compared.

suspicious TDLNs with metastasis, the shortest diameter or SUVmax of the two largest TDLNs was used to compare the changes in size or tumor metabolism before and after treatment.

Neoadjuvant immunotherapy

Neoadjuvant therapy-related information, such as agents, courses, doses, and duration of final neoadjuvant treatment to surgery,[25,26] was collected and summarized in Supplementary Methods and Table S1.

Operation and TDLNs dissection

After completion of neoadjuvant treatment, 18F-FDG PET-CT or whole-body examination was performed to evaluate therapeutic response and resectability, preferably 2 weeks after the last dose of therapy. Then, patients who did not have disease progress underwent surgery, given that radiographic evaluation poorly reflects the truly pathologic response after ICIs.[1,25] Posterolateral thoracotomy (open) or video-assisted thoracic surgery (VATS) with systemic lymphadenectomy, routinely covering N1 (≥ 3 stations) and N2 (≥ 3 stations), was performed.[27] N1 refers to a lymph node metastasis to a peribronchial or ipsilateral hilar lymph node; N2 represents a lymph node metastasis to an ipsilateral mediastinal lymph node and/or a subcarinal lymph node. Clinical and pathologic staging of patients were judged according to the American Joint Committee on Cancer (AJCC) Lung Cancer Staging (8th edition). TDLNs status was classified as TDLNs+ or TDLNs-, based on the absence or presence of metastatic tumor cells after ICIs treatment.

All patients received postoperative adjuvant immunotherapy or immuno- chemotherapy after a discussion with the multidisciplinary tumor board was carried out.

Smoking and PD-L1 subgroups

Cumulative smoking exposure was determined in terms of pack-years by multiplying the number of years smoked with the average number of packs per day. Based on pack-years of smoking, participants were classified as never smokers (0.0 pack-years), light-moderate smokers (0.1–40.0 pack-years), and heavy smokers (> 40 pack-years).[25,28] Tumoral PD-L1 expression from the clinical records (retrospectively reviewed) was scored by a senior pathologist according to the programmed death-ligand 1 (PD-L1) tumor proportions score (TPS) before neoadjuvant immunotherapy, and samples were divided into 3 subgroups: high (≥50%), moderate [1-50%), and low (< 1%) PD-L1.

Treatment response assessments

The neoadjuvant treatment response, retrospectively reviewed of the clinical records, was assessed based on the Response Evaluation Criteria in Solid Tumors (RECIST; version 1.1). Of note, in this study, to analyze the impact of TDLNs status on the therapeutic response of the primary tumor beds ("tumor bed" refers to the area where the pretreatment tumor was originally located) to neoadjuvant ICIs, we separately analyzed the pathologic responses of primary lung tumor beds and paired TDLNs, given that in lymph node metastases, it is often difficult to assess tumor stromal inflammation owing to the background lymphocytes.[29] Overall, the pCR referred to the absence of viable tumor cells (ypT0NxM0) in the surgically resected primary tumors; MPR was defined as 10% or less viable tumor cells in the surgically resected primary tumors. pCR/MPR in the primary tumors and TDLNs were referred to as pCR-P/MPR-P and pCR-LN/MPR-LN, respectively.

Histopathologic evaluation

Histopathologic data were retrieved from the clinical records. Besides, hematoxylin and eosin (H&E)-stained slides of paraffin-embedded sections of the primary tumor and paired TDLNs were additionally retrospectively reviewed by one senior pathologist blinded to the patients' treatments and outcomes. The final histopathologic evaluation would be then determined.

Regarding the histopathologic examination of the primary tumor beds, multiple sections of the tumor bed (including the longest diameter) were entirely sampled.[29] In this study, the number of tumor slides per sample ranged from 4 to 7, which is dependent on the residual tumor size. Generally, the 5–7 slides (median: 6) that almost cover entire primary tumors were used for histologic examination if the size was small (< 3 cm), in that small size is associated with dramatic tumor shrinkage and fewer tumor residuals (good response) after neoadjuvant treatment, thus requiring careful examinations. For tumors with a large size (≥ 3 cm) that is commonly related to more tumor cell residuals (poor response) after neoadjuvant treatment, it is easy to detect the residual tumor cells with a smaller number of slides (median: 5). Concerning the lymph nodes, the TDLNs were entirely examined if the size was small (1.0 cm) in the longest diameter. The number of lymph node slides ranged from 3 to 5.

The evaluation of primary tumor response was performed as previously described: % of residual tumor = viable tumor area/total tumor bed area, whereby the total tumor bed = residual viable tumors + regression bed + necrosis.[30,31]

Multiplexed immunofluorescence staining, image acquisition and data quantification

Serial 5-μm tissue sections from the matched resected TDLNs+ and TDLNs- were deparaffinized, rehydrated, pretreated for antigen retrieval, and then stained with hematoxylin and eosin and subjected to multiplexed

immunofluorescence staining (see the detailed information in the Supplementary Methods). The primary antibodies used were listed in Table S1.

For HE and common IHC sections, whole slide images were acquired using Grundium Ocus® microscope scanners, as previously described. The staining intensities of cancer and stromal cells in the images of full tissue sections were automatically analyzed and quantified using QuPath open-source software (version 0.3.2), where the DAB channel intensity of stained markers (membrane, cytoplasm or nuclear OD value according to their intracellular locations) was extracted for each section.[32,33] For the classification of cancer cells, stromal cells, and necroptosis, multiple training regions representing typical morphologies of cancer and stromal cells as well as necroptotic regions are annotated first. Based on this, the unique parameters of each cell type were generated, which were then applied to the whole slide images.

For multiplexed IF, slides were scanned and imaged using the Pannoramic MIDI® platform and were analyzed in batches using QuPath open-source software (version 0.3.2) for the quantification of positively stained cells as previously described. Consequently, we were able to quantify the positively-stained cells with one or combination markers. With this, we know how many cells are positive for single (e.g., CD8+ only), double (e.g., PD1+CD8+), or triple (e.g., CD19 +CD11c+CD21+) staining, as described previously.[34,35] For the spatial staining analysis in this study, we selected TDLN+ and paired TDLN- from 6 LUSC patients, including pCR (n=2), MPR (n=2), and non-pCR/MPR (n=2) in the primary tumor beds. Of note, for the case selection, we excluded the TDLNs that have been almost completely taken up by the metastatic tumor cells, because there is no sufficient material in the adjacent lymph node area to analyze.

Follow-up, events definition and survival time analysis

The first follow-up visit was scheduled 4 weeks after discharge. Adjuvant therapies were then typically started 1 month postoperatively. Later, follow-up visits were scheduled every 3 months. Follow-up information was obtained from patients by telephone calls or clinic revisit records. No patients were lost to follow-up in this cohort.

The survival time is defined as the time from the day of surgical removal of the primary tumor to the occurrence of the events (tumor recurrence or patients' death) or the date of last follow-up (at the end of March 2022). The survival time of patients who have not experienced the events by the time of the last follow-up was defined as censoring. Specifically, recurrence-free survival (RFS) was defined as the interval between the day of surgery and the date of detected tumor relapse by any cause or the last follow-up date. Overall survival (OS) was defined as the interval between the day of surgery and the date of death by any cause or the last follow-up date.

Statistical analysis

Data were analyzed from January 2018 to December 2021. Normally distributed continuous variables are presented as mean ± SD; otherwise, they are presented as median and range. Categorical variables are shown as numbers and percentages. Baseline characteristics were compared between tumors with TDLNs+ or TDLNs- cohorts by using chi-square or Fisher's exact test (expected frequencies < 5) for categorical data.

Multivariable Logistic regression (by generalized linear model [GLM] function in R software) was used to adjust the relevant variables to get the association between the specific factor of interest and the measurement outcomes (e.g., pathologic status in the TDLNs (TDLNs+ vs. TDLNs-) and/or pathologic response in the primary tumor beds (pCR/MPR-P vs. non-pCR/MPR-P)). Similarly, the multivariable Cox proportional-hazards model (using the "survminer" and "survival" R packages) was used to adjust the relevant variables to get the predictive effects of some specific factors of interest on survival. For the Cox proportional-hazards model, the proportional hazard (PH) assumption is generally tested (Schoenfeld residuals) at first. If the PH assumption is met (p-value > 0.05) and there is no intersection between the two groups-represented lines, we consider the hazards are proportional over time; otherwise, we perform the analysis only during time periods when the PH assumption is met. Strategies used for the selection of variables included in the multivariable analysis (Logistic or Cox regression model) were as follows: 1) the variables found to be significant on invariable analysis (defined as potential confounders and determined by a probability value of less than 0.2); 2) clinically relevant factors that have been reported to influence the measurement outcomes (TDLNs status after ICI treatment, response of the primary tumor beds, or patients' survival), e.g., sex, age, smoking history, clinical tumor stage, tumor histology, resection type, and treatment regimens (immunotherapy alone vs. chemo-immunotherapy); 3) among the above candidates, variables whose frequency is less than 5 in any comparative subgroups will be excluded; 4) finally, the above selected variables in the multivariable analysis models will be further modified to exclude the intermediate variables (mediators) and thus achieve the minimal sufficient adjustment sets by drawing the directed acyclic graph (DAG).[36] There was no formal sample size calculation in this study, and the sample size in this study was determined according to the previous simulation study, recommending that Logistic and Cox models should be used with 5-9 outcome events per predictor variable (EPV).[37] Since we included 9 variables in our study, thus a minimum of 45 samples were needed to detect the association of the influencing factors and measurement outcomes in each model. Data summary and statistical analysis were performed using R software (version 3.4.1). A p-value < 0.05 was considered statistically significant.

Role of the funding source

This work was supported by the National Natural Science Foundation of China (82072570 to F. Yao; 82002941 to B. Sun), the excellent talent program of Shanghai Chest Hospital (to F.Y), the Basic Foundation Program for Youth of Shanghai Chest Hospital (2021YNJCQ2 to H.Yang), and the Innovative Research Team of High-level Local Universities in Shanghai (SHSMU-ZLCX20212302 to F. Yao). The funder had no any role in study design, data collection, data analysis, interpretation, or writing of report.

Results

Neoadjuvant ICIs induce differential radiological changes between primary tumor beds and paired TDLNs

A total of 68 patients with locally-advanced NSCLCs who received neoadjuvant immunotherapy or chemo-immunotherapy followed by surgery were included in this study. The clinicopathologic characteristics were shown in Table 1. Of those, 32 had pathologically-confirmed residual tumor cells in the TDLNs after ICIs

	Factors	TDLNs+	TDLNs-	p-value
n		32	36	
Sex (%)	Female	6 (18.8)	0 (0.0)	0.022
	Male	26 (81.2)	36 (100.0)	
Age (mean (SD))		58.12 (7.44)	61.22 (7.94)	0.103
Smoking History (%)	Heavy	4 (12.5)	13 (36.1)	0.076
	Light-Moderate	17 (53.1)	15 (41.7)	
	Never	11 (34.4)	8 (22.2)	
Pretreatment tumor size (mean (SD))		4.82 (2.10)	4.81 (2.08)	0.984
PD-L1 TPS (%)	$\geq$ 50%	4 (28.6)	11 (64.7)	0.03
	1-49%	9 (64.3)	3 (17.6)	
	$\leq$ 1%	1 (7.1)	3 (17.6)	
Clinical stage (%)	IIB	1 (3.1)	4 (11.1)	0.325
	IIIA	22 (68.8)	21 (58.3)	
	IIIB	8 (25.0)	7 (19.4)	
	IIIC	1 (3.1)	4 (11.1)	
Location (%)	LL	2 (6.2)	5 (13.9)	0.283
	LU	8 (25.0)	4 (11.1)	
	RL	9 (28.1)	8 (22.2)	
	RM	1 (3.1)	0 (0.0)	
	RU	12 (37.5)	19 (52.8)	
Histology (%)	LUAD	9 (28.1)	7 (19.4)	0.164
	LUSC	22 (68.8)	23 (63.9)	
	Other	1 (3.1)	6 (16.7)	
Neoadjuvant regimens (%)	ICIs alone	5 (15.6)	3 (8.3)	0.579
	ICIs plus Chemotherapy	27 (84.4)	33 (91.7)	
Resection types (%)	Bilobectomy	5 (15.6)	3 (8.3)	0.144
	Lobectomy	23 (71.9)	23 (63.9)	
	Pneumonectomy	2 (6.2)	1 (2.8)	
	Sleeve	2 (6.2)	9 (25.0)	
Surgical approach (%)	Open	8 (25.0)	11 (30.6)	0.811
	VATS	24 (75.0)	25 (69.4)	
Resection (%)	R0	29 (90.6)	36 (100.0)	0.198
	R1	3 (9.4)	0 (0.0)	
Response of primary tumor beds (%)	Non-pCR/MPR-P	17 (53.1)	9 (25.0)	0.012
	MPR-P	10 (31.2)	10 (27.8)	
	pCR-P	5 (15.6)	17 (47.2)	
No. of resected TDLN stations (mean (SD))		7.47 (1.61)	6.72 (1.80)	0.077
No. of resected TDLNs (mean (SD))		16.03 (6.65)	15.61 (9.26)	0.832

***Table 1*: Invariable analysis of clinical factors associated with pathologic status of TDLNs.**

ICI: immune checkpoint inhibitors; PD-L1: Programmed death-ligand 1; TPS: tumor proportions score; TDLNs: Tumor-draining lymph nodes; TDLNs+: tumor invaded; TDLNs-: tumor-free; LL: left lower; LU: left upper; RL: right lower; RU: right upper; LUAD: lung adenocarcinoma; LUSC: lung squamous cell carcinoma; VATS: video-assisted thoracoscopic surgery; R0: radical resection; R1: microscopically positive resection margin; pCR-P: pathological complete response in the primary tumor beds.; MPR-P: pathological major response in the primary tumor beds.

treatment (TDLNs+ group), and the remaining 36 had tumor-free TDLNs (TDLNs- group). The median number of resected TDLN stations in this study cohort was 7 (≥ 3 N1 stations and ≥ 3 N2 stations), covering an average of 15.8 nodes per case. Of the TDLNs+ cases, the majority (17 of 32, 53.1%) have residual tumor cells in both N1 and N2 nodes, followed by 10 cases with N1 nodes involvement only and 5 cases with N2 nodes involvement only.

After neoadjuvant ICIs, the response patterns in the primary tumor beds and paired TDLNs were characterized by comparing the pre- and post-treatment radiological images. The results showed that there was a significant reduction in the radiological size of the primary tumor beds after neoadjuvant ICIs treatment, which was independent of the degree of therapeutic responses in the primary tumor beds or the pathologic status of the TDLNs (Figure 2a). In contrast to the primary tumor beds, neoadjuvant ICIs treatment was overall associated with a significant enlargement of the radiographic size of abnormal TDLNs (the definition of abnormal TDLNs could be found in the Methods section) (Figure 2b). Intriguingly, subgroup analysis demonstrated that the enlargement predominantly exists in patients who achieved MPR/pCR-p, but not in those with non-MPR/pCR-P (Figure 2b). These observations suggested that radiographic changes in the size of primary tumor beds could not well discriminate pathologically good responders (MPR/pCR-P) from poor responders, which was in line with previous evidence demonstrating a poor discordance between the image-guided and pathologic evaluation of the response to ICIs in lung tumors.[1,25] Notably, the observed increase in the size of abnormal TDLNs after neoadjuvant ICI treatment occurs primarily in MPR-P/pCR-P (Figure 2b). This argues against the feasibility of using radiographic size changes in TDLNs as a parameter for judging the response to ICI treatment, which is typically included to evaluate the therapy response based on the widely-used RECIST (v1.1) criteria.[38] Conversely, pseudoprogression, as indicated by enlargement of abnormal TDLNs after neoadjuvant ICIs treatment, appears to be associated with better therapeutic effects of ICIs in the primary tumors, which warrants further validation.

Primary lung tumor beds and paired TDLNs exhibit distinct metabolic responses to neoadjuvant ICIs therapy

18F-FDG PET-CT, reflecting the metabolic activity of glucose uptake, is widely used as a powerful tool for the diagnosis of malignancies. Also, in the clinic, PET-CT is a sensitive and indispensable tool to detect the presence of TDLNs metastasis in various cancer types. More importantly, considerable evidence has shown that PET-CT could greatly facilitate the evaluation of treatment response to neoadjuvant chemotherapy or chemo-radiotherapy in lung cancer.[39] However, evidence that compares the 18F-FDG-reflected metabolic changes of the primary tumor beds and their paired TDLNs is lacking.

In this cohort, we were able to analyze the metabolic changes of the primary tumor beds and their paired TDLNs in 12 patients that had the matched pre- and post-treatment PET-CT data. Interestingly, we observed a significant decline in the 18F-FDG uptake (indicated by the SUVmax value) in MPR/pCR-P but not in their non-MPR/pCR-P counterparts (Figure 2c). Additional subgroup analysis based on the status of TDLNs showed that TDLN- subgroup was associated with a significantly lower metabolic activity in its paired primary tumor bed, which, however, was not observed in the TDLN+ subgroup (Figure 2c). Concerning the TDLNs, we observed that neoadjuvant ICI treatment induces a dramatic decrease in the metabolic activity of the TDLNs-, but not in the TDLNs+ subgroup (Figure 2d). Furthermore, changes in the metabolic activity of the TDLNs are irrespective of the pathologic responses in their paired primary tumor beds (Figure 2d). Notably, in some cases whose primary tumor beds have a pCR or MPR, there is a prominent increase in the metabolic activity of the paired TDLNs after ICI treatment (Figure 2d, e; Supplementary Fig. 1a). These lines of evidence suggested that TDLNs and their paired primary tumor beds vary widely in response to ICIs treatment. Particularly, the tumor-free status of TDLNs, namely TDLNs-, appears to have a significant and positive impact on the metabolic response of their paired primary tumors to ICIs (Figure 2c).

In some other cases, only pre- or post-ICIs PET-CT data are available. We then integrated these data and separately analyzed the association of pre- or post-ICIs SUVmax values with pathologic responses in the primary tumor beds or abnormal TDLNs. Interestingly, the analyses showed that the MPR/pCR-P events were only significantly related to the SUVmax value of the primary tumor beds after rather than before treatment (Figure 2f), and were also regardless of the TDLNs status (Supplementary Fig. 1b). These observations highlighted the post-ICIs SUVmax in the primary tumor beds as a potential indicator of the degree of pathologic responses. The optimal cut-off value of post-ICIs SUVmax to distinguish MPR/pCR-P from non-MPR/pCR-P in this study population was 11.5 (sensitivity: 0.83; specificity: 0.90) (Figure 2g), which requires further studies with a large cohort.

In sum, neoadjuvant ICIs induce differential radiological and metabolic changes between primary tumor and paired TDLNs, which also has distinct implications for the therapy response in the primary lesions of lung cancer.

TDLNs+ cases are associated with poor response to neoadjuvant ICIs in the primary tumor beds

We next sought to investigate the differences in the clinicopathological characteristics between TDLNs+ and

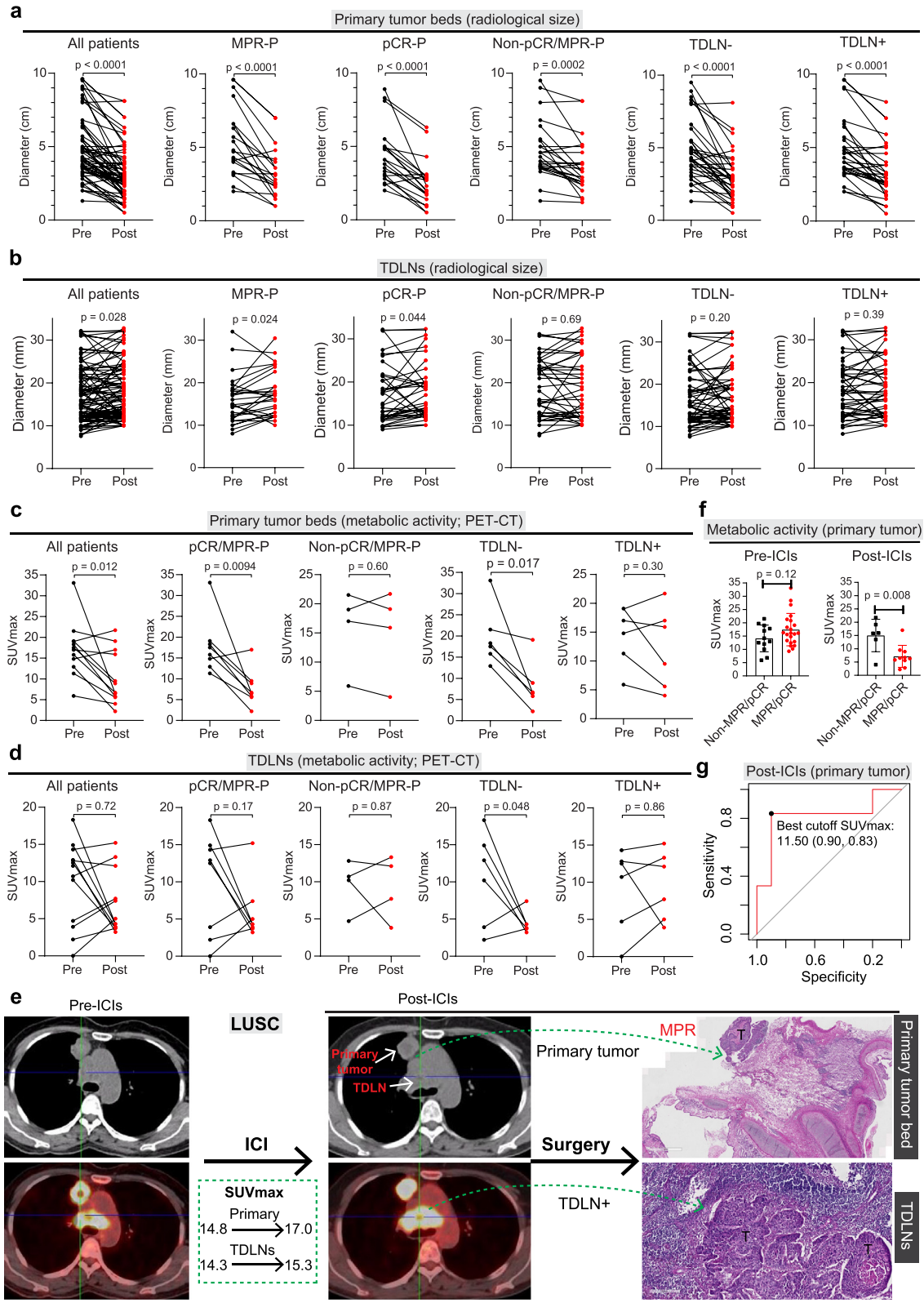

Figure 2. ICIs induced different changes in the radiological size and metabolic activity in primary tumor beds and paired TDLNs. a, b, ICIs-induced changes in the radiological size in the primary tumor beds (a) or paired abnormal tumor-draining lymph nodes (TDLNs) (b). pCR-P: pathological complete response in the primary tumor beds; MPR-P: major pathological response in the

TDLNs- subgroups after surgery. Compared with TDLNs- group, the TDLNs+ group had a significantly higher proportion of female patients, a lower frequency of high PD-L1 score (TPS ≥ 50%) in the pretreatment biopsies, and poorer response (lower incidence of pCR/MPR-P and higher incidence of non-pCR/MPR-P) to ICIs (Table 1; Figure 3a, b). Recent biological experimental evidence has verified that TDLN and immune response in the paired primary tumors are reciprocally interplayed,[3,5,19,40] we then sought to know how much these two factors affect each other. After adjusting for the confounding factors (age, smoking, clinical stage, resection type and No. of resected TDLN stations) based on the DAG (Supplementary Fig. 2a), multivariable logistic regression analysis identified that pCR/MPR-P occurrence was associated with a significantly lower risk of TDLNs+ events (odds ratio [OR] = 0.26; 95% confidence interval [CI]: 0.086−0.77) (Table 2). Likewise, based on the multivariable logistic analysis that adjusts for the potential confounders (age, smoking, clinical stage, resection type and No. of resected TDLN stations) (Supplementary Fig. 2b), the occurrence of TDLNs+ was associated with significantly lower risk of pCR/MPR-P events in the primary tumor beds (OR = 0.27; 95%CI: 0.09−0.79) (Table 3; Table S3;). Remarkably, a higher number of invaded TDLNs was associated with a greater frequency of non-pCR/MPR-P (Figure 3c). Together, these results implied that the presence of TDLNs+ appeared to negatively affect the ICIs response in the primary tumor beds of lung cancer, which was in conformity with the above metabolic response data (Figure 2c).

Notably, 22.7% (5 of 22) of cases with pCR-P (Figure 3a), suggesting that tumor cells in the TDLNs+ have different therapeutic responses to the same ICI treatment, compared to their paired primary tumors, which reinforces the above idea that primary tumor beds exhibit different response patterns from their paired TDLNs (Figure 2). Also, these observations suggest that metastatic tumors within TDLNs+ might represent a special population capable of evading immune surveillance and developing resistance to ICIs treatment, consequently leading to the failure of ICIs and tumor relapse.

The presence of TDLNs+ after neoadjuvant ICIs treatment predicts a poor post-surgical prognosis

Next, we sought to know the association between TDLNs status after neoadjuvant ICIs treatment and the post-surgical prognosis of these patients. In this cohort, one case died on postoperative day 29 due to the bronchopleural fistula and was excluded for subsequent survival analysis. The median follow-up time was 806 days (range 133−1399 days). At the end of follow-up, 23.9% (16 of 67) patients had a tumor relapse, and 17.9% (12 of 67) patients died, including 3 with MPR-P and 2 with pCR-P. Three-year RFS and OS were 70.0% and 79.0%, respectively (Figure 4a).

Overall, the presence of TDLNs+ after neoadjuvant ICIs treatment was associated with significantly shorter RFS compared with that of TDLN- cases (Figure 4b). Furthermore, multivariable Cox analysis identified the presence of TDLNs- was significantly (hazard ratio [HR] = 0.20; 95%CI: 0.051−0.76) associated with longer RFS after adjusting for the covariates (age, smoking, clinical stage, resection type, response of the primary tumor beds, and No. of resected TDLN stations) (Supplementary Fig. 3a; Figure 4c). There is a trend toward a longer OS in the TDLN- cases, although the difference did not reach a statistical significance (Figure 4b; Supplementary Fig. 3b, 3c), which might be due to the small sample size and short follow-up duration. Therefore, further studies are required to investigate the impact of TDLNs+ on the long-term prognosis of patients receiving neoadjuvant ICIs.

More importantly, even in the cases with pCR-P, we also observed the presence of TDLNs+ as an unfavorable factor for RFS and OS (Figure 4d), suggesting that its predictive role is not related to the degree of the response of primary tumor beds to ICIs treatment. These observations indicated that the residual tumor cells within TDLNs+ after neoadjuvant ICIs treatment represent a potentially critical source of tumor relapse. Besides, a high PD-L1 TPS score was also associated with a better prognosis (Figure 4e).

Metastatic colonization in TDLNs+ is associated with T cells exclusion

TDLNs are enriched for various immune components, most of which are T and B cells. Beyond the immune

primary tumor beds. TDLN+ represents TDLNs with residual tumor cells (metastatic), and TDLN- indicates tumor-free TDLNs. Of note, some of these cases with had a size smaller than 10 mm have underwent biopsy, confirming the presence of TDLNs metastasis. As such, in Figure 2b, we could be able to see that some dots are under 10 mm (y-axis, diameter). p-value was calculated using a paired two-sided t-test. c, d, ICIs-induced changes in the metabolic activity (indicated by the SUVmax value on 18F-FDG PET-CT) in the primary tumor beds (c) and paired abnormal TDLNs (d). *p*-value was calculated using a paired two-sided t-test. e, Representative conventional CT and 18F-FDG PET-CT images showing that ICIs induced an increase in the metabolic activity (indicated by the SUVmax value on 18F-FDG PET-CT) in one LUSC case with MPR-P. On the right, H&E staining showing ICIs induced MPR in the primary tumor beds but not in the paired abnormal TDLNs. f, The association of SUVmax value measured on the pre-ICIs (left) or post-ICIs (right) primary tumors samples (not paired) with the pathologic response in the primary tumor beds. *p*-value was calculated using an unpaired two-sided t-test. g, Operating characteristic curve (ROC) analysis showing to determine the best cut-off of post-ICIs SUVmax value in predicting pathologic responses in the primary tumor beds. Here, 0.9 represents the sensitivity, and 0.83 indicates the specificity.

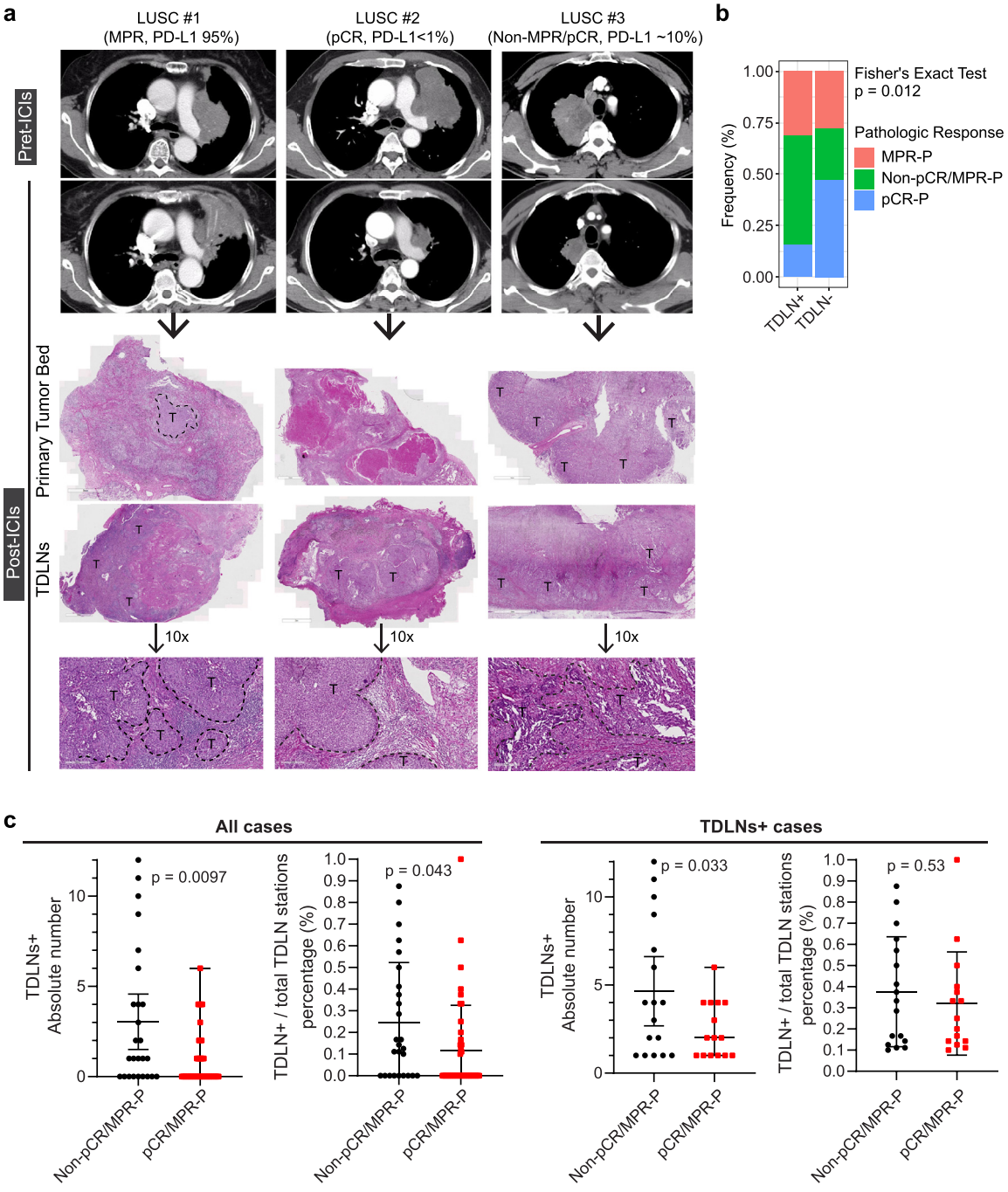

Figure 3. The presence of TDLNs+ is related to a poor response in their paired primary tumor beds. a, Representative CT and H&E images before (pre-ICIs) and after (post-ICIs) neoadjuvant immune checkpoint inhibitors (ICIs). Three lung squamous cell carcinoma (LUSC) cases with different degrees of pathologic response were shown. T stands for tumor region. pCR-P: pathological complete response in the primary tumor beds; MPR-P: major pathological response in the primary tumor beds. Scale bar: 200 μm. b, The association between pathologic response (pCR-P, MPR-P, non-pCR/MPR-P) of the primary tumor beds and the pathologic status of paired tumor-draining lymph nodes (TDLNs: TDLNs+ vs. TDLNs-). TDLN+ represents TDLNs with residual tumor cells (metastatic), and TDLN- indicates tumor-free TDLNs. c, The association between pathologic response (pCR/MPR-P vs. non-pCR/MPR-P) and the number (absolute number of resected nodes and the number of resected nodal stations) of invaded TDLNs across the entire cohort (left) or TDLNs+ cases (right). *p*-value was calculated using an unpaired two-sided t-test.

Exposure variable of primary interest:	Adjusted OR[a] (95%CI)	Pr(>|z|)
Response of primary tumor beds (pCR/MPR-P vs. Non-pCR/MPR-P)	0.26 (0.086−0.77)	0.016[b]

***Table 2*: Adjusted association between the primary tumor response and the pathologic state of TDLNs (TDLNs+ vs. TDLNs-) after neoadjuvant ICI therapy.**

OR: odds ratio; CI: confidence interval; TDLNs: Tumor-draining lymph nodes; ICI: immune checkpoint inhibitors. pCR-P: pathological complete response in the primary tumor beds; MPR-P: pathological major response in the primary tumor beds.; -P: -primary tumor beds.

[a] The adjusted analysis was done via a design-based binary logistic regression analysis (refer to the directed acyclic graph (DAG) in Figure S2a), adjusted for age (<60 yrs vs. ≥60 yrs), smoking (ever vs. never), clinical stage (IIIB-IIIC vs. II-IIIA), resection type (standard vs. extended lobectomy) and No. of resected TDLN stations (<8 vs. more). Here, the factor "Sex" was not included because their sample size in the subgroups was too small (less than 5 cases).

[b] Significant.

Exposure variable of primary interest:	Adjusted OR[a] (95%CI)	Pr(>|z|)
Pathologic nodal status (TDLNs+ vs. TDLNs-)	0.27 (0.09−0.79)	0.017[b]

***Table 3*: Adjusted association between the pathologic status of TDLNs and primary tumor responses (pCR/MPR-P vs. non-pCR/MPR-P) after neoadjuvant ICI therapy.**

OR: odds ratio; CI: confidence interval; TDLNs: Tumor-draining lymph nodes; ICI: immune checkpoint inhibitors. pCR-P: pathological complete response in the primary tumor beds; MPR-P: pathological major response in the primary tumor beds.; -P: -primary tumor beds.

[a] The adjusted analysis was done via a design-based binary logistic regression analysis (refer to the drawing and analyzing causal diagrams (DAG) in Figure S2b), adjusted for age (<60 yrs vs. ≥60 yrs), smoking (ever vs. never), clinical stage (IIIB-IIIC vs. II-IIIA), resection type (standard vs. extended lobectomy) and No. of resected TDLN stations (<8 vs. more).

[b] Significant.

cells, components within the stromal compartment of TDLNs, e.g., HEVs, (FRCs) and follicular dendritic cells, have also been demonstrated to play critical roles in complementing the proper functions of antitumor immunity.[19,21] ICIs can reinvigorate the exhausted immune cells and/or also enhance the recruitment of immune cells from the peripheral circulation. However, there are few studies characterizing the immune and non-immune compartments between the TDLNs- and TDLNs+ after neoadjuvant ICIs therapy.

We then performed mIF staining analysis by including lymphocyte markers (CD4, CD8, FOXP3 [regulatory T cells], CD19 [B cells]), HEVs [peripheral node addressin (PNAd); also known as MECA-79][41]), conventional dendritic cells (CD11c),[22] follicular dendritic cells (CD21),[42] and the immune checkpoint protein (PD-1).

Characterization of T cells (co-staining CD8 and PD1) showed that CD8+ T cells were mostly distributed around but rarely infiltrating into the metastatic lesions within the TDLNs+ despite the neoadjuvant ICIs treatment (Figure 5a, 5b; Supplementary Fig. 4a), although the density of CD8+ T cells in their adjacent intact LN region (without tumor involvement) was much higher than that within the paired TDLNs- (Figure 5b). The total number of CD8+ T cells (per tissue slice) within TDLNs+ was much lower than their paired TDLNs- (Figure 5b). These observations suggest that the infiltration of T cells into metastatic lesions within TDLNs+ was drastically restricted. Notably, in TDLNs+ after ICIs treatment, only a small percentage (mean: 4.9%) of those peritumoral CD8+ T cells co-express PD-1, and the number of PD-1+ T cells in the adjacent LN region within the TDLNs+ is comparable to that within the paired TDLNs- (Figure 5c; Supplementary Fig. 4b), suggesting that their inability to infiltrate into the metastatic lesions was less likely due to the exhaustion of CD8+ T cells.

Similarly, we observed that CD4+ T cells were also mainly located around with few penetrating into the metastatic foci within TDLNs+ (Figure 5d, 5e). There is no difference in the density of CD4+ T cells in the adjacent intact LN region (without tumor involvement), whereas the total number of CD4+ T cells (per tissue slice) within TDLNs+ was much lower than their paired TDLNs- (Figure 5e, 5e). Importantly, TDLNs+ had more FOXP3+CD4+ T cells in the peritumoral intact LN region, compared with the paired TDLNs- counterparts (Figure 5d, 5e), which is in line with previous evidence demonstrating the accumulation of immunosuppressive FOXP3+ Treg cells within the TDLNs.[43] Besides, CD19+ B cells were more abundant in TDLNs- (Figure 5f; Supplementary Fig. 4c).

TDLNs+ are associated with abnormal HEVs, diminished FDCs and cDCs

Trafficking of lymphocytes into tumors is critical for antitumor immunity and the efficacy of ICIs.[4,19] High endothelial venules (HEVs) function as a route for immune cell trafficking/transmigration,[19,41] and are believed to increase primed T cell infiltration to enhance antitumor T cell immunity. Characterizing the HEVs within TDLNs demonstrated that the morphology of HEVs surrounding the metastatic lesions was highly compressed and collapsed (Figure 6a), evidenced by a significantly narrower diameter, compared with that of

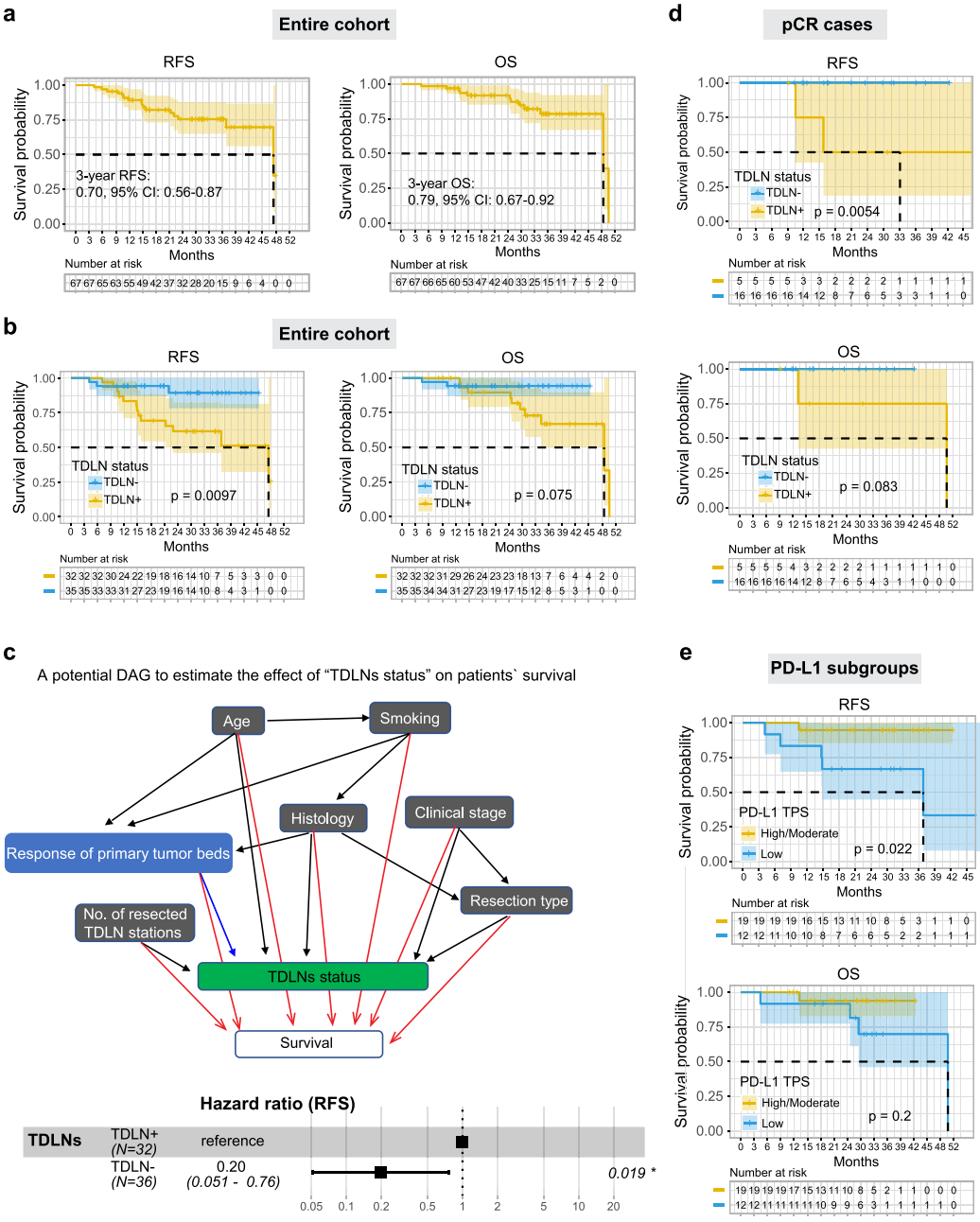

Figure 4. The presence of TDLNs+ is predictive of poor post-surgical survival. a, b, Recurrence−free survival (RFS; left) and overall survival (OS; right) of patients receiving neoadjuvant immunotherapy in the entire cohort (A) and TDLN+/TDLN- subgroups (b). TDLN+ represents TDLNs with residual tumor cells (metastatic), and TDLN- indicates tumor-free TDLNs. c, Multivariable COX analysis showing the predictive effects of TDLNs status on the RFS in patients receiving neoadjuvant immunotherapy in the entire cohort. The adjusted analysis was done via illustrating a directed acyclic graph (DAG; upper panel), adjusted for age (<60 yrs vs. ≥60 yrs), smoking (ever vs. never), clinical stage (IIIB-IIIC vs. II-IIIA), resection type (standard vs. extended lobectomy), primary tumor response (pCR/MPR-P vs. Non-pCR/MPR-P) and No. of resected TDLN stations (<8 vs. more). The proportional hazard assumption was met before the Cox regression analysis (refer to Figure S3a, 3b). d, RFS (upper) and OS (lower) of patients receiving neoadjuvant immunotherapy in cases with pCR (pathological complete response) in the primary tumor beds. TDLN+ represents TDLNs with residual tumor cells (metastatic), and TDLN- indicates tumor-free TDLNs. e, RFS (upper) and OS (lower) of patients receiving neoadjuvant immunotherapy in cases with different programmed death-ligand 1 (PD-L1) tumor proportions score (TPS) in the primary tumor beds. TDLN+ represents TDLNs with residual tumor cells (metastatic), and TDLN- indicates tumor-free TDLNs.

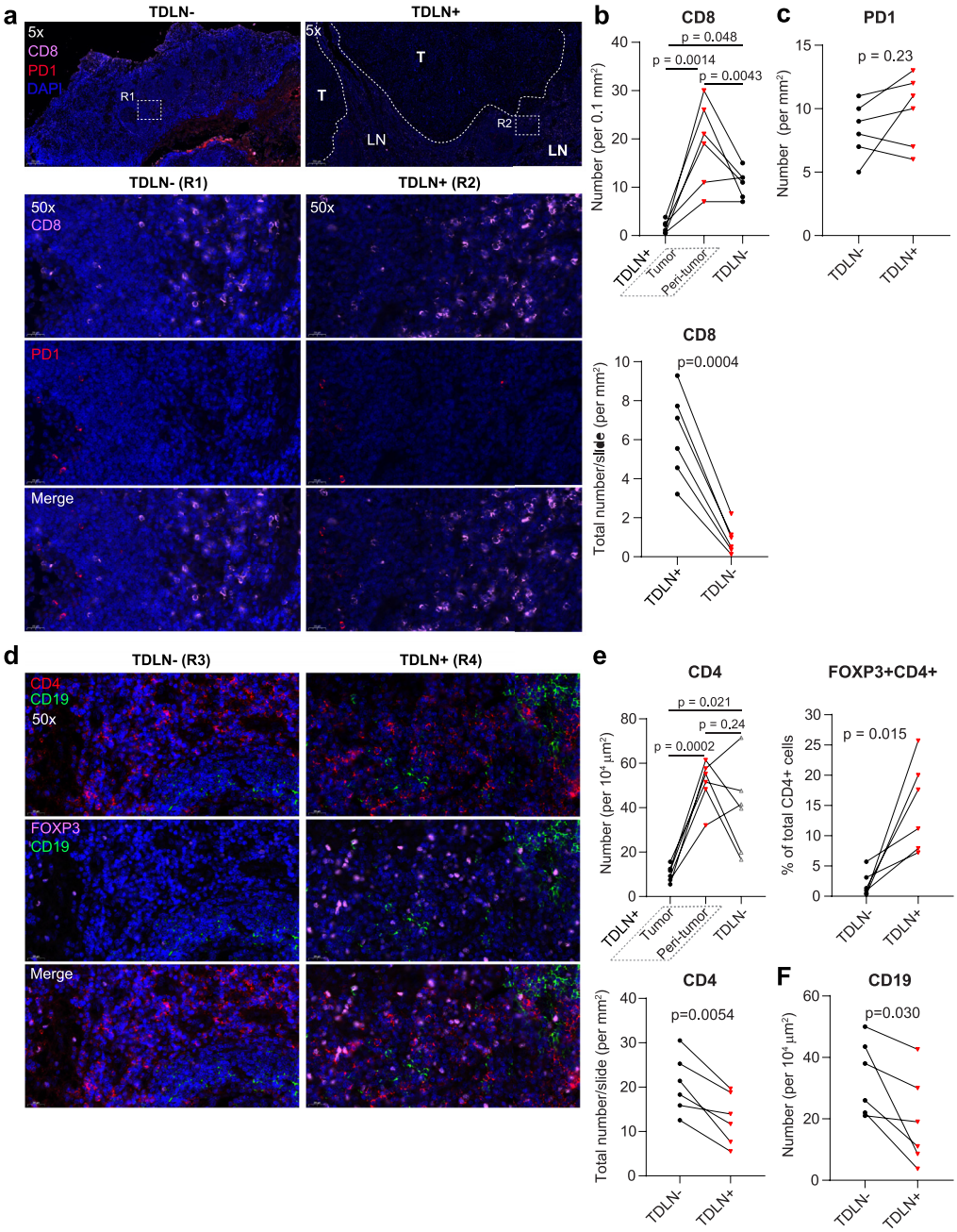

Figure 5. Comparing the immune cell profiling between TDLNs- and paired TDLNs+. a, Representative CD8 co-staining with PD1 in a TDLN- and its paired TDLN+ of a resected LUSC (lung squamous cell carcinoma) (ypT2aN2M0) case. The image acquisition of all markers occurred simultaneously. T stands for tumor region; LN stands for adjacent intact lymph node region. R1 and R2 represent the selected regions from the TDLN- and TDLN+ samples, respectively. Scale bar: 200 μm (5x, upper panel) and 20 μm (50x, lower panel). b, c, Quantification of CD8+ (b) or PD1+ (c) cells between TDLNs- and their paired TDLNs+ across 6 LUSC samples of this cohort. The quantification was performed by using QPath software (see the methods). Peri-tumor indicates the intact LN regions surrounding the metastatic lesions of TDLNs+. *p*-value was calculated using a paired two-sided t-test. d, Representative triple staining of CD4, FOXP3, CD19 in a TDLN- and its paired TDLN+ (related to a). The image acquisition of all markers occurred simultaneously. R3 (related to Supplementary Fig. 3B) and R4 (related to Supplementary Fig. 3B) represent the selected regions from the TDLN- and TDLN+ samples, respectively. Scale bar: 20 μm (50x). e, f, Quantification of CD8+ (b) or PD1+ (c) cells between TDLNs- and their paired TDLNs+ across 6 LUSC samples of this cohort. The quantification was performed by QPath software (see the methods). Peri-tumor indicates the intact LN regions surrounding the metastatic lesions of TDLNs+. *p*-value was calculated using a paired two-sided t-test.

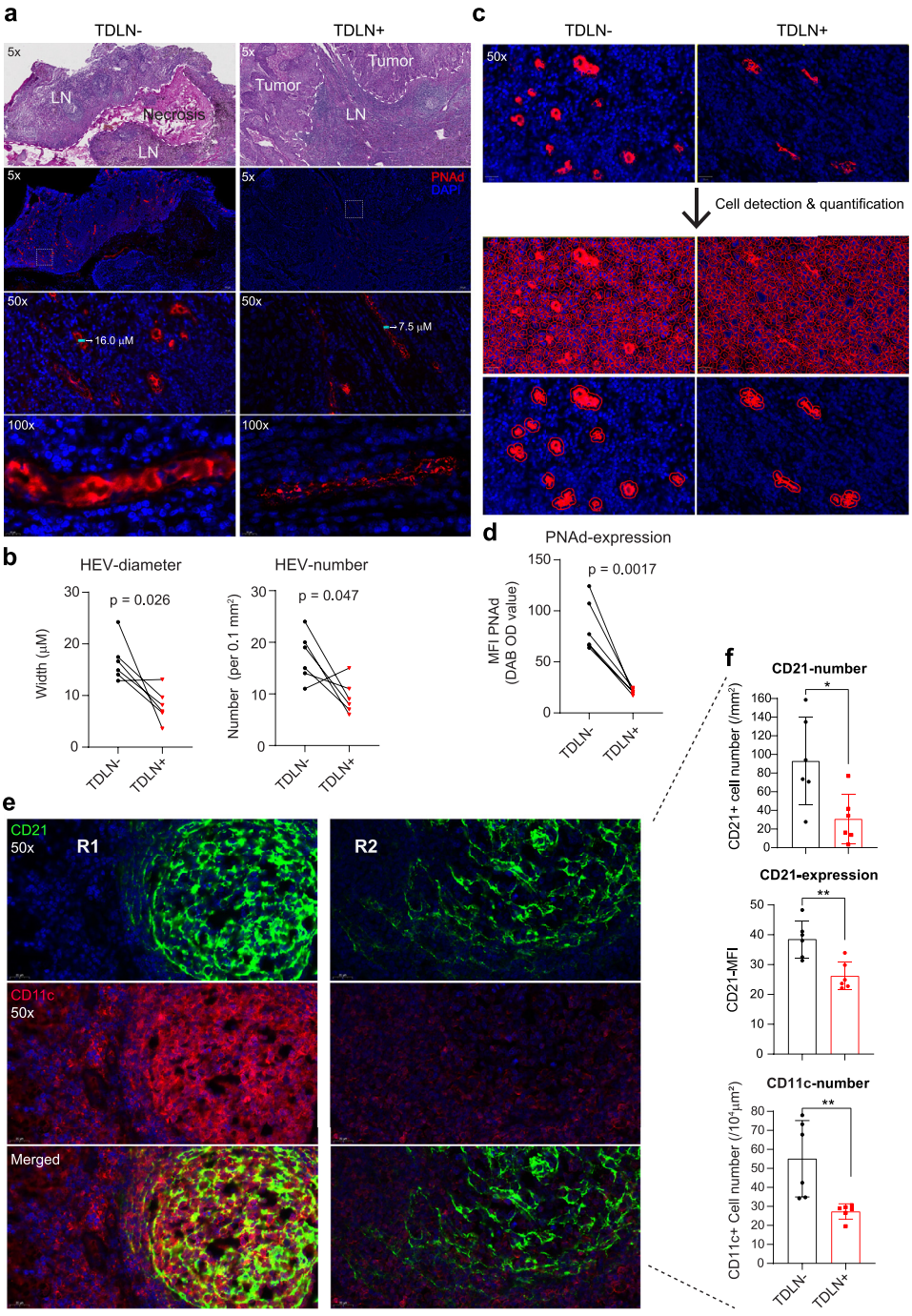

Figure 6. TDLNs+ are associated with reduced expression of HEVs, FDCs and cDCs. a-d, Characterization of high endothelial venules (HEVs) between TDLNs- and TDLNs+. Representative H&E and PNAd staining (a, c) in a TDLN- and its paired TDLN+ of a resected LUSC (lung squamous cell carcinoma) (ypT2aN2M0) case. LN stands for adjacent intact lymph node region. The quantifications (number and diameter of HEVs in b; HEVs expression (MFI: mean fluorescence intensity) in d) across 6 LUSC samples of this cohort were shown in b. The middle and lower panels in c showing the artificial intelligence-based recognition of all single cells and PNAd+ HEVs, respectively, by implementing QPath software. p-value was calculated using a paired two-sided t-test. Scale bar: 200 μm (5x, upper panel), 20 μm (50x, middle panel), and 10 μm (100x, lower panel). e, f, Characterization of CD21 (marking follicular dendritic cells (FDCs)) and CD11c (marking conventional dendritic cells (cDCs)) between TDLNs- and TDLNs+. R1 (related to Supplementary Fig. 4) and R2 (related to Supplementary Fig. 4) represent the selected regions from the TDLN- and TDLN+ samples, respectively. *p*-value was calculated using a paired two-sided t-test. Scale bar: 20 μm (50x).

their paired TDLNs- (Figure 6b). Furthermore, the density of HEVs within the TDLNs+ was significantly reduced (Figure 6b). Since the mean fluorescence intensity (MFI) of PNAd staining can well reflect the quality of HEVs and their degree of maturity/functionality,[44] we then quantified the MFI and discovered that the mean MFI of PNAd was significantly diminished in TDLNs+ than their TDLNs- counterparts (Figure 6c, 6d). These observations indicated that the metastatic lesions within TDLNs+ might cause a deformity/dysfunction of HEVs, consequently leading to impaired access of primed lymphocytes to the primary lung tumor beds, which might be related to poor pathologic response of the primary tumor beds in the aforementioned TDLNs+ cases (Figure 3; Table 2, 3).

Follicular dendritic cells (FDCs) are another critical subset within the stromal compartment of TDLNs and are typically located within the B cell follicles and germinal centers of LNs. FDCs are essential for B cell response that present antigen to B cells, and are fundamentally different from conventional dendritic cells (cDCs) in lineage and function.[45] After neoadjuvant ICIs, we discovered that adjacent intact LN regions within the TDLNs+ were characterized by a significant reduction of FDCs and cDCs, compared with their TDLN- counterparts (Figure 6e, 6f; Supplementary Fig. 5).

Together, these data suggested that metastatic lesions within TDLNs+ might remodel the stromal compartment, which might also partly contribute to the impaired mobilization of anti-tumor immune response mediated by TDLNs.

Discussion

TDLNs represent pivotal organs for antitumor immunity[5] and play key roles in mediating the efficacy of ICIs therapy.[3,19,20,46] Although a variety of factors are linked with resistance to ICIs,[47] few studies have investigated the association between TDLNs metastasis, which is frequently observed in the clinic, and therapy resistance/failure of ICIs in lung cancer. Moreover, studies characterizing the immune profiling between TDLNs+ and TDLNs- in the case of ICIs treatment are lacking. More critically, the mechanisms involved in this process are unknown. Our study uncovered an underappreciated role of TDLNs+ in restraining the therapeutic response of their paired primary lung tumors and the differential cellular compositions between TDLNs+ and their paired TDLNs-, which further advances our understanding of the TDLNS as an essential part of effective ICIs treatment in lung cancer.

The role of TDLNs in tumor immunity and response to ICIs

Although recent evidence highlights the essential role of TDLNs in determining the efficacy of ICIs,[3,6,7] the evidence was mainly based on preclinical mouse models of other cancer types. The relationship between TDLNs status and therapeutic response to ICIs has not been well characterized in clinical lung cancer patients. Surgery following neoadjuvant ICIs treatment provides an ideal setting and a unique opportunity to answer that question, in that primary tumor and regional TDLNs can be simultaneously resected and investigated.[25] In our study cohort, we found that 4 out of 22 cases with pCR-P had pathologically-confirmed metastatic lesions within the matched TDLNs, especially in the N2 lymph nodes, which was associated with worse survival after neoadjuvant immunotherapy plus surgery (Figure 4). These observations suggest that the residual tumor cells could not only escape the immune surveillance to migrate to TDLNs but also develop resistance to ICIs, which defines a special scenario of dysfunctional antitumor immunity that was incapable to elicit effective antitumor immunity.

Multiple components including the immune and non-immune cells within the micro-ecosystem of TDLNs might be involved. resident memory or progenitor CD8+ T cells have been reported to be the key tumor-specific lymphocytes mediating the anti-tumor immunity.[20,22,48] Beyond that, growing attention has been recently paid to HEVs that are specialized vessels that allow lymphocyte recirculation through the TDLNs and are indispensable for effective ICI therapy.[19,49,50] In this study, we discovered that the number and expression (MFI) of HEVs within the TDLNs+ were drastically reduced, compared with TDLNs- (Figure 6a, 6b). Besides, HEVs within TDLNs are malformed. In line with this, recent evidence showed that solid stresses could remodel HEVs in TDLNs+, resulting in the exclusion of lymphocytes in the metastatic lesions.[51] In addition, other immune cells, e.g., B cells, conventional DCs, and non-immune cells, e.g., FRCs, which also play a role in facilitating the immune response,[3,19–22] are declined within the TDLNs+ (Figure 6c, 6d).

A better knowledge of the pathobiology of TDLNs metastasis would assist to devise new intervention strategies aimed at harnessing TDLNs to augment the efficacy of cancer immunotherapy.

The utility of PET-CT in predicting the pathologic response to ICIs

PET-CT has been routinely used in clinical for malignant diagnosis and detection of TDLNs metastasis, as well as evaluation of treatment response. In lung cancer, a poor consistency between the histopathologic examination and radiological evaluation on the treatment response of primary tumor beds to ICIs has been extensively reported.[1,25] However, we found that in the setting of neoadjuvant ICIs, PET-CT provides certain values in evaluating the therapeutic effects on tumor response in the primary tumor beds but not in the

TDLNs. In this cohort, we observed an enlarged size of the abnormal TDLNs after neoadjuvant ICIs specifically in cases that have MPR/pCR-P (Figure 2b). These observations raised an important issue on the PET-CT-based evaluation of the pathologic response in the TDLNs, which are also incorporated for the evaluation of therapy responses based on the broadly-used RECIST v1.1 guideline. Our observations were supported by several other studies.[24,25,52,53] Concerning the metabolic activity, in contrast with the primary tumor beds, we observed an increasing trend in the SUVmax value after neoadjuvant ICIs (Figure 2b), which was independent of the degree of pathologic response in the matched primary tumor beds. This was also supported by a recent study.[52] Notably, this phenomenon was shown to be specific to ICIs other than chemotherapy.[52] Thus, it is critical to identify effective strategies to precisely determine the pathologic response in the TDLNs before surgery, particularly those with pCR-P, in that surgery might be avoided after ICIs.

18F-FDG PET-CT reflects the metabolic activity of tumors mainly via measuring glucose uptake because tumor cells are thought to consume considerably higher glucose than normal cells to support their unlimited growth. Why the SUVmax value in tumor-free TDLNs after ICIs therapy increases has not been investigated. Strikingly and surprisingly, a recent study demonstrated that myeloid cells had the greatest capacity to take up intratumoral glucose, followed by T cells and cancer cells.[54] In contrast, cancer cells mainly take up glutamine and lipids instead.[54] These findings might explain the increased uptake of glucose in the TDLNs after ICIs therapy, which leads to a highly inflammatory response.[24,25,52] Thus, glutamine rather than glucose-based PET-CT imaging might facilitate the treatment response of ICIs.[55]

Systematic versus selective resection of TDLNs following neoadjuvant ICIs

During curative surgery, the TDLNs are routinely and systematically resected to provide accurate staging, confirm complete resection, predict the prognosis, and determine the need for postoperatively adjuvant therapy. Accordingly, in the clinical practice of NSCLC surgery, it is recommended to resect a minimum of 6 nodal stations, including 3 from N2 (the mediastinum, in particular, the subcarinal node (#7)) and 3 from N1 zones.[27] This standard surgical procedure has been long established for many years. Interestingly, recent clinical evidence in melanoma[56] and breast cancer[57] patients did not support the routine use of completion dissection of regional LNs, as completion dissection could not improve the prognosis in these patients. Thus, whether the indiscriminate resections of all TDLNs will compromise the benefits from subsequent ICIs needs to be reconsidered, given that emerging evidence has highlighted TDLNs as the most critical site for the generation of effective tumor-specific T cell response.[3,20,46,48]

Recently, a retrospective study encompassing 5117 patients with clinical stage I-III NSCLC demonstrated that a less rigorous TDLNs resection was associated with significantly better 5-year RFS and OS.[58] These findings reinvoke our thoughts on the necessity of unselective TDLNs resection, particularly in the setting of immunotherapy. Notably, studies from other groups have shown in pre-clinical models that TDLNs play a pivotal role in PD-1/PD-L1-based immunotherapy, and that surgical resection of TDLNs before treatment hampers therapeutic outcomes.[7,59] In agreement, recent evidence points to the need for the recruitment of newly primed effector T cells outside of the tumor microenvironment to ensure the efficacy of ICIs.[3,4]

The above evidence raises concerns that how to perform surgical removal of TDLNs in NSCLC patients treated with neoadjuvant ICIs. In our study cohort, we observed that in some cases with pCR at the primary tumor beds, there are still residual tumor cells in the TDLNs. Thus, an optimal way is to selectively resect the TDLNs with residual tumors but keep intact tumor-free TDLNs to preserve the regional immunity for subsequent adjuvant ICI therapy. A prerequisite for such a surgical strategy requires a reliable indicator to specifically localize the metastatic TDLNs pre- or intra-operation.[60]

Conclusions

Overall, TDLNs+ represent a special scenario where the antitumor immunity is drastically suppressed. The role of TDLNs has long been overlooked, and therapeutic targeting of abnormal TDLNs may promote sufficient activation of antitumor T cells and their subsequent tumor infiltration to ensure effective ICIs. A comprehensive understanding of the mechanisms underpinning cancer migration and growth in TDLNs is the key to overcoming the resistance to ICIs and developing an effective therapy for the eradication of TDLN metastases, which requires further studies.

The major limitations of our study include the small sample size, and that the cases for neoadjuvant ICIs treatment were highly selected by a multidisciplinary team. Besides, we did not have PD-L1 expression data and genetic information of the primary tumors and/or paired TDLNs across all cases, given that PD-L1 expression and the presence of some frequently mutated genes in LUSC, e.g., *KEAP1/NFE2L2*, are also related to the response to ICIs. Another potential issue is that we did not separately analyze the differences in the immune cell profiling of TDLNs between paired primary tumor beds with different degrees of response, due to the very limited sample size. Also, it is better to utilize more markers to more precisely define the identity of immune cells within TDLNs. Moreover, before

neoadjuvant ICIs treatment, the TDLNs status was not pathologically confirmed in all samples, which might affect the accurate clinical staging judgment and subsequent analysis of the association between TDLNs status and ICI therapy response, thus prospective clinical studies are warranted.

Contributors

Conceptualisation: H.Y. and F.Y.; Data curation: Y.H., B.S., W.M., L.F., K.X. and Y.J.; Formal analysis: H.Y. and B.S., W.M.; Investigation: H.Y., B.S., W.M., L.F., K. X. and Y.J. This study was conceived, designed, and interpreted by H.Y. and F.Y.; Methodology: H.Y.; Project administration: F.Y. and Z.W.; Software: H.Y.; Supervision: F.Y. and Z.W.; Writing – original draft: H. Y., B.S., and W.M. critically reviewed the manuscript; H.Y., F.Y., Z.W and J.X. had primary responsibility for the final content; All authors read, revised and approved the final manuscript.

Data sharing statement

The authors declare that all the data supporting the findings in this study are available in this study and its Supplementary materials, or are available from the corresponding author through reasonable request.

Declaration of interests

The authors declare that they have no conflict of interest.

Acknowledgments

We thank Tissue Biobank Department and the Pathology Department (Shanghai Chest Hospital, Shanghai Jiao Tong University) for providing the sample materials and pathological analysis of the treatment response in the samples. This work was supported by the National Natural Science Foundation of China (82072570 to F. Yao; 82002941 to B. Sun), the excellent talent program of Shanghai Chest Hospital (to F.Y), the Basic Foundation Program for Youth of Shanghai Chest Hospital (2021YNJCQ2 to H.Yang), and the Innovative Research Team of High-level Local Universities in Shanghai (SHSMU-ZLCX20212302 to F. Yao).

Supplementary materials

Supplementary material associated with this article can be found in the online version at doi:10.1016/j.ebiom.2022.104265.

References

1 Forde PM, Chaft JE, Smith KN, et al. Neoadjuvant PD-1 blockade in resectable lung cancer. *N Engl J Med*. 2018;378(21):1976–1986.
2 Boyero L, Sanchez-Gastaldo A, Alonso M, Noguera-Ucles JF, Molina-Pinelo S, Bernabe-Caro R. Primary and Acquired resistance to immunotherapy in lung cancer: unveiling the mechanisms underlying of immune checkpoint blockade therapy. *Cancers (Basel)*. 2020;12(12):3729.
3 O'Melia MJ, Manspeaker MP, Thomas SN. Tumor-draining lymph nodes are survival niches that support T cell priming against lymphatic transported tumor antigen and effects of immune checkpoint blockade in TNBC. *Cancer Immunol Immunother*. 2021;70(8):2179–2195.
4 Wu TD, Madireddi S, de Almeida PE, et al. Peripheral T cell expansion predicts tumour infiltration and clinical response. *Nature*. 2020;579(7798):274–278.
5 du Bois H, Heim TA, Lund AW. Tumor-draining lymph nodes: at the crossroads of metastasis and immunity. *Sci Immunol*. 2021;6(63):eabg3551.
6 Francis DM, Manspeaker MP, Schudel A, et al. Blockade of immune checkpoints in lymph nodes through locoregional delivery augments cancer immunotherapy. *Sci Transl Med*. 2020;12(563).
7 Fransen MF, Schoonderwoerd M, Knopf P, et al. Tumor-draining lymph nodes are pivotal in PD-1/PD-L1 checkpoint therapy. *JCI Insight*. 2018;3(23):e124507.
8 Schneider JL, Rowe JH, Garcia-de-Alba C, Kim CF, Sharpe AH, Haigis MC. The aging lung: physiology, disease, and immunity. *Cell*. 2021;184(8):1990–2019.
9 Bienenstock J. The lung as an immunologic organ. *Annu Rev Med*. 1984;35:49–62.
10 Wu Y, Han C, Gong L, et al. Metastatic patterns of mediastinal lymph nodes in small-size non-small cell lung cancer (T1b). *Front Surg*. 2020;7:580203.
11 Goldstraw P, Chansky K, Crowley J, et al. The IASLC lung cancer staging project: proposals for revision of the TNM stage groupings in the forthcoming (eighth) edition of the TNM classification for lung cancer. *J Thorac Oncol*. 2016;11(1):39–51.
12 Quinn JJ, Jones MG, Okimoto RA, et al. Single-cell lineages reveal the rates, routes, and drivers of metastasis in cancer xenografts. *Science*. 2021;371(6532):eabc1944.
13 Pereira ER, Kedrin D, Seano G, et al. Lymph node metastases can invade local blood vessels, exit the node, and colonize distant organs in mice. *Science*. 2018;359(6382):1403–1407.
14 Brown M, Assen FP, Leithner A, et al. Lymph node blood vessels provide exit routes for metastatic tumor cell dissemination in mice. *Science*. 2018;359(6382):1408–1411.
15 Ginsberg RJ, Rubinstein LV, Lung Cancer Study Group. Randomized trial of lobectomy versus limited resection for T1 N0 non-small cell lung cancer. *Ann Thorac Surg*. 1995;60(3):615–622. discussion 22-3.
16 Lim E, Baldwin D, Beckles M, et al. Guidelines on the radical management of patients with lung cancer. *Thorax*. 2010;65(suppl 3):iii1–iii27.
17 Ubellacker JM, Tasdogan A, Ramesh V, et al. Lymph protects metastasizing melanoma cells from ferroptosis. *Nature*. 2020;585(7823):113–118.
18 Lee CK, Jeong SH, Jang C, et al. Tumor metastasis to lymph nodes requires YAP-dependent metabolic adaptation. *Science*. 2019;363(6427):644–649.
19 Asrir A, Tardiveau C, Coudert J, et al. Tumor-associated high endothelial venules mediate lymphocyte entry into tumors and predict response to PD-1 plus CTLA-4 combination immunotherapy. *Cancer Cell*. 2022;40(3):318–334.e9.
20 Connolly KA, Kuchroo M, Venkat A, et al. A reservoir of stem-like CD8(+) T cells in the tumor-draining lymph node preserves the ongoing antitumor immune response. *Sci Immunol*. 2021;6(64):eabg7836.
21 Krishnamurty AT, Turley SJ. Lymph node stromal cells: cartographers of the immune system. *Nat Immunol*. 2020;21(4):369–380.
22 Schenkel JM, Herbst RH, Canner D, et al. Conventional type I dendritic cells maintain a reservoir of proliferative tumor-antigen specific TCF-1(+) CD8(+) T cells in tumor-draining lymph nodes. *Immunity*. 2021;54(10):2338–2353.e6.
23 Spicer J, Wang C, Tanaka F, et al. Surgical outcomes from the phase 3 CheckMate 816 trial: Nivolumab (NIVO) + platinum-doublet chemotherapy (chemo) vs chemo alone as neoadjuvant treatment for patients with resectable non-small cell lung cancer (NSCLC). *J Clin Oncol*. 2021;39(15_suppl):8503.
24 Ling Y, Li N, Li L, et al. Different pathologic responses to neoadjuvant anti-PD-1 in primary squamous lung cancer and regional lymph nodes. *NPJ Precis Oncol*. 2020;4(1):32.
25 Yang H, Ma W, Sun B, et al. Smoking signature is superior to programmed death-ligand 1 expression in predicting pathological

response to neoadjuvant immunotherapy in lung cancer patients. *Transl Lung Cancer Res*. 2021;10(9):3807–3822.
26 Xu K, Yang H, Ma W, et al. Neoadjuvant immunotherapy facilitates resection of surgically-challenging lung squamous cell cancer. *J Thorac Dis*. 2021;13(12):6816–6826.
27 Asamura H, Chansky K, Crowley J, et al. The international association for the study of lung cancer lung cancer staging project: proposals for the revision of the N descriptors in the forthcoming 8th edition of the TNM classification for lung cancer. *J Thorac Oncol*. 2015;10(12):1675–1684.
28 Lee YH, Shin MH, Kweon SS, et al. Cumulative smoking exposure, duration of smoking cessation, and peripheral arterial disease in middle-aged and older Korean men. *BMC Public Health*. 2011;11:94.
29 Travis WD, Dacic S, Wistuba I, et al. IASLC multidisciplinary recommendations for pathologic assessment of lung cancer resection specimens after neoadjuvant therapy. *J Thorac Oncol*. 2020;15(5):709–740.
30 Weissferdt A, Pataer A, Vaporciyan AA, et al. Agreement on major pathological response in NSCLC patients receiving neoadjuvant chemotherapy. *Clin Lung Cancer*. 2020;21(4):341–348.
31 Pataer A, Weissferdt A, Vaporciyan AA, et al. Evaluation of pathologic response in lymph nodes of patients with lung cancer receiving neoadjuvant chemotherapy. *J Thorac Oncol*. 2021;16(8):1289–1297.
32 Bankhead P, Loughrey MB, Fernandez JA, et al. QuPath: open source software for digital pathology image analysis. *Sci Rep*. 2017;7(1):16878.
33 Yang H, Liang SQ, Xu D, et al. HSP90/AXL/eIF4E-regulated unfolded protein response as an acquired vulnerability in drug-resistant KRAS-mutant lung cancer. *Oncogenesis*. 2019;8(9):45.
34 Yang H, Sun B, Fan L, et al. Multi-scale integrative analyses identify THBS2(+) cancer-associated fibroblasts as a key orchestrator promoting aggressiveness in early-stage lung adenocarcinoma. *Theranostics*. 2022;12(7):3104–3130.
35 Wang L, Yang H, Dorn P, et al. Peritumoral CD90+CD73+ cells possess immunosuppressive features in human non-small cell lung cancer. *EBioMedicine*. 2021;73:103664.
36 Westreich D, Greenland S. The table 2 fallacy: presenting and interpreting confounder and modifier coefficients. *Am J Epidemiol*. 2013;177(4):292–298.
37 Vittinghoff E, McCulloch CE. Relaxing the rule of ten events per variable in logistic and Cox regression. *Am J Epidemiol*. 2007;165(6):710–718.
38 Schwartz LH, Litiere S, de Vries E, et al. RECIST 1.1-Update and clarification: From the RECIST committee. *Eur J Cancer*. 2016;62:132–137.
39 Pottgen C, Gauler T, Bellendorf A, et al. Standardized uptake decrease on [18F]-fluorodeoxyglucose positron emission tomography after neoadjuvant chemotherapy is a prognostic classifier for long-term outcome after multimodality treatment: secondary analysis of a randomized trial for resectable stage IIIA/B non-small-cell lung cancer. *J Clin Oncol*. 2016;34(21):2526–2533.
40 Reticker-Flynn NE, Zhang W, Belk JA, et al. Lymph node colonization induces tumor-immune tolerance to promote distant metastasis. *Cell*. 2022;185(11):1924–1942.e23.
41 Lee M, Kiefel H, LaJevic MD, et al. Transcriptional programs of lymphoid tissue capillary and high endothelium reveal control mechanisms for lymphocyte homing. *Nat Immunol*. 2014;15(10):982–995.
42 Wang X, Cho B, Suzuki K, et al. Follicular dendritic cells help establish follicle identity and promote B cell retention in germinal centers. *J Exp Med*. 2011;208(12):2497–2510.
43 Deng L, Zhang H, Luan Y, et al. Accumulation of foxp3+ T regulatory cells in draining lymph nodes correlates with disease progression and immune suppression in colorectal cancer patients. *Clin Cancer Res*. 2010;16(16):4105–4112.
44 Moussion C, Girard JP. Dendritic cells control lymphocyte entry to lymph nodes through high endothelial venules. *Nature*. 2011;479(7374):542–546.
45 Fletcher AL, Acton SE, Knoblich K. Lymph node fibroblastic reticular cells in health and disease. *Nat Rev Immunol*. 2015;15(6):350–361.
46 van Pul KM, Fransen MF, van de Ven R, de Gruijl TD. Immunotherapy goes local: the central role of lymph nodes in driving tumor infiltration and efficacy. *Front Immunol*. 2021;12:643291.
47 Havel JJ, Chowell D, Chan TA. The evolving landscape of biomarkers for checkpoint inhibitor immunotherapy. *Nat Rev Cancer*. 2019;19(3):133–150.
48 Molodtsov AK, Khatwani N, Vella JL, et al. Resident memory CD8 (+) T cells in regional lymph nodes mediate immunity to metastatic melanoma. *Immunity*. 2021;54(9):2117. 32.e7.
49 Park HS, Kim YM, Kim S, et al. High endothelial venule is a surrogate biomarker for T-cell inflamed tumor microenvironment and prognosis in gastric cancer. *J Immunother Cancer*. 2021;9(10):e003353.
50 Menzel L, Zschummel M, Crowley T, et al. Lymphocyte access to lymphoma is impaired by high endothelial venule regression. *Cell Rep*. 2021;37(4):109878.
51 Jones D, Wang Z, Chen IX, et al. Solid stress impairs lymphocyte infiltration into lymph-node metastases. *Nat Biomed Eng*. 2021;5(12):1426–1436.
52 Cascone T, Weissferdt A, Godoy MCB, et al. Nodal immune flare mimics nodal disease progression following neoadjuvant immune checkpoint inhibitors in non-small cell lung cancer. *Nat Commun*. 2021;12(1):5045.
53 Gao S, Li N, Gao S, et al. Neoadjuvant PD-1 inhibitor (Sintilimab) in NSCLC. *J Thorac Oncol*. 2020;15(5):816–826.
54 Reinfeld BI, Madden MZ, Wolf MM, et al. Cell-programmed nutrient partitioning in the tumour microenvironment. *Nature*. 2021;593(7858):282–288.
55 Dunphy MPS, Harding JJ, Venneti S, et al. In vivo PET assay of tumor glutamine flux and metabolism: in-human trial of (18)F-(2S,4R)-4-fluoroglutamine. *Radiology*. 2018;287(2):667–675.
56 Faries MB, Thompson JF, Cochran AJ, et al. Completion dissection or observation for sentinel-node metastasis in melanoma. *N Engl J Med*. 2017;376(23):2211–2222.
57 Giuliano AE, Ballman KV, McCall L, et al. Effect of axillary dissection vs no axillary dissection on 10-year overall survival among women with invasive breast cancer and sentinel node metastasis: the ACOSOG Z0011 (Alliance) randomized clinical trial. *JAMA*. 2017;318(10):918–926.
58 Lee J, Hong YS, Cho J, et al. Reclassifying the International Association for the Study of Lung Cancer Residual Tumor Classification According to the Extent of Nodal Dissection for NSCLC: One Size Does Not Fit All. *J Thorac Oncol*. 2022;17(7):890–899.
59 Chamoto K, Chowdhury PS, Kumar A, et al. Mitochondrial activation chemicals synergize with surface receptor PD-1 blockade for T cell-dependent antitumor activity. *Proc Natl Acad Sci USA*. 2017;114(5):E761–EE70.
60 Cao F, Guo Y, Li Y, et al. Fast and accurate imaging of lymph node metastasis with multifunctional near-infrared polymer dots. *Adv Funct Mater*. 2018;28(16):1707174.